Catal Lett (2009) 127:419–428
DOI 10.1007/s10562-008-9723-y

Rare Earth Pyrophosphates: Effective Catalysts for the Production of Acrolein from Vapor-phase Dehydration of Glycerol

Qingbo Liu · Zhen Zhang · Ying Du · Jing Li · Xiangguang Yang

Received: 1 August 2008 / Accepted: 6 October 2008 / Published online: 11 November 2008
© Springer Science+Business Media, LLC 2008

Abstract Vapor-phase dehydration of glycerol to produce acrolein was investigated at 320 °C over rare earth (including La, Ce, Nd, Sm, Eu, Gd, Tb, Ho, Er, Tm, Yb, Lu) pyrophosphates, which were prepared by precipitation method. The most promising catalysts were characterized by means of XRD, FT-IR, TG-DTA, BET and NH_3-TPD measurements. The excellent catalytic performance of rare earth pyrophosphate depends on the appropriate surface acidity which can be obtained by the control of pH value in the precipitation and the calcination temperature, e.g. $Nd_4(P_2O_7)_3$ precipitated at pH = 6 and calcined at 500 °C in the catalyst preparation.

Keywords Glycerol · Acrolein · Alcohol dehydration · Rare earth pyrophosphates · Solid acid

1 Introduction

In recent years, much attention has been devoted to applying green catalytic processes to convert biorenewable feedstock to commodity chemicals and clean fuels because of the threat of depletion of petroleum and global warming [1–4]. Glycerol (1, 2, 3-propanetriol) which can be found naturally in the form of fatty acid esters, is widely available and rich in functionalities. Acrolein is an important and versatile chemical intermediate and raw material for the production of acrylic acid esters, super absorber polymers or detergents. Catalytic conversion of glycerol to acrolein could be an important route for using glycerol resources and could offer a cost effective and sustainable alternative to the currently commercial catalytic petrochemical process based on the oxidation of propylene over a Bi/Mo-mixed oxide catalyst.

Various solid acid catalysts including sulphates, phosphates and zeolites have been tested for the dehydration of glycerol in either gaseous or liquid phases [5–7]. An acrolein yields up to 75% at complete conversion of glycerol were obtained at 250–340 °C over acidic ZSM-5 or HY zeolites as the catalysts [6]. On the other hand, dehydration of glycerol was also carried out in supercritical water with liquid acids or salts as catalysts [8, 9]. Acrolein selectivity up to 80% at 90% conversion was reported with H_2SO_4 as catalyst at 400 °C [10]. Recently, Chai et al. communicated the use of sulphated zirconia [11] or Nb_2O_5 [12] but these catalysts did not show better performance. Tsukuda et al. [13] tested heteropolyacids supported over SiO_2 and found that the introduction of mesopores in silica support significantly affected the catalytic activity. Atia et al. [14] found that alumina was superior to silica as support material with regard to catalyst activity and selectivity when heteropolyacid as the active compounds. However, such strongly acidic catalysts deactivate quickly as carbonaceous deposits block the catalyst surface, particularly in the presence of large amounts of micropores. Otherwise, the catalyst deactivation is also caused by the dissolution of heteropolyacids from support, especially in aqueous solution. Therefore, it is necessary to develop a high efficient and stable catalyst for the dehydration of glycerol to produce acrolein.

Q. Liu · Z. Zhang · Y. Du · J. Li · X. Yang (✉)
Laboratory of Green Chemistry and Process, Changchun Institute of Applied Chemistry, Chinese Academy of Sciences, Changchun 130022, People's Republic of China
e-mail: xgyang1@eyou.com

Q. Liu · Z. Zhang · Y. Du · J. Li · X. Yang
Graduate School of the Chinese Academy of Sciences, Beijing, People's Republic of China

Many transition metal pyrophosphates including SnP_2O_7, ZrP_2O_7, TiP_2O_7, $(VO)_2P_2O_7$, CeP_2O_7, $Cu_2P_2O_7$ and $Mn_2P_2O_7$ have been studied in oxydehydrogenation of *n*-butane [15–19], oxidation of benzyl alcohol [20], and oxidation of Benzene to Phenol [21]. Besides, rare earth pyrophosphates used as solid acid catalysts have been reported by our group [22] recently. In this paper we report our investigations on the catalytic behavior of rare earth pyrophosphates catalysts in the vapor-phase dehydration of glycerol to produce acrolein. The effects of pH value and calcination temperature in the preparation on the acidic property of the catalyst and the catalytic performance in the vapor-phase dehydration of aqueous glycerol have also been discussed in detail. Though a lot of rare earth pyrophosphates have been tested in this work, only the most promising catalyst $Nd_4(P_2O_7)_3$ was emphasized.

2 Experimental

2.1 Catalyst Preparation

Rare earth pyrophosphates were synthesized by precipitation method. The typical preparation process as following: 0.01346 mol $Na_4P_2O_7 \cdot 10H_2O$ and 0.01794 mol rare earth nitrate were dissolved separately in 100 mL H_2O. Then the sodium pyrophosphate solution was dropped into the rare earth nitrate solution with stirring and kept stirring for an additional 18 h after precipitation. The precipitate was recovered by filtering off, washing, and dried at 110 °C for 12 h. After calcined at 500 °C for 3 h, the samples were pressed, crushed and sieved to 40–60 mesh before use.

In order to regulate the pH value of the solution, HNO_3 was added while the $Nd_4(P_2O_7)_3$ catalysts were synthesized by the precipitation method, the $Nd_4(P_2O_7)_3$ catalysts precipitated in the condition of pH = 4, 5, 6, and 7 were denoted as NP-n (n = 4, 5, 6 and 7 respectively).

2.2 Characterizations

The powder X-ray diffraction (XRD) data were obtained by using an X-ray diffract meter (D/MAXIIB, Rigaku), operating at 40 kV and 10 mA, using Cu Ka radiation combined with Nickel filter. The samples were scanned in the range of 2θ = 10–70° at a scanning rate of 3°/min.

FT-IR spectra were taken on the instrument BRUKER Vertex 70 FTIR by using KBr wafers with the resolution of 1 cm^{-1}.

Thermal analyses (TG-DTA) of rare earth pyrophosphates, as well as temperature-programmed oxidation (TPO) measurements of the used catalysts, were conducted on a TA Instruments SDT Q600 thermal analyzer. The sample was placed in an α-Al_2O_3 cumber and heated in flowing air (100 mL/min) from 50 °C to 750 °C at a rate of 15 °C/min. Before the measurements, the samples were dried overnight at 110 °C.

The specific surface areas of the samples were measured by using Mircomeritics ASAP 2010. The specific surface areas of the calcined samples were determined from N_2 adsorption conducted at −196 °C by using high vacuum volumetric sorbometric glass system. Prior to the adsorption measurement the sample was degassed at 300 °C for 4 h under a reduced pressure of 10^{-5} Torr.

NH_3-TPD spectra were performed on a homemade apparatus equipped with an on-line QIC-20 quadrupole mass spectrometer (Hiden Analytical Ltd) as detector. After treated at 550 °C for 1 h and cooled to 100 °C in helium atmosphere, the sample was exposed to 20 mL/min NH_3 for 30 min, and then swept with helium at a rate of 30 mL/min; finally the sample was heated at a rate of 10 °C/min in helium to collect the NH_3-TPD data.

2.3 Catalytic Reaction

The vapor-phase dehydration of glycerol was conducted at 320 °C under atmospheric pressure in a vertical fixed-bed quartz reactor (8 mm i.d.) using 1 mL of catalyst. Before the reaction, the catalyst was pretreated at 320 °C for 2 h in flowing dry N_2 (30 mL/min). The reaction feed, an aqueous solution containing 36.2 wt.% glycerol (molar ratio glycerol/water = 1/9), was fed into the reactor by a micropump at a space velocity (GHSV) of glycerol of 227 h^{-1}. The reaction products were condensed in a dry ice-ethanol trap and collected hourly for analysis by GC equipped with a DM-5 (Dikma, 30 m) capillary column and a flame ionization detector. The condensed products during the first hour of the reaction were abandoned due to the poor material balance.

3 Results and Discussion

3.1 Catalyst Characterization

3.1.1 XRD and FTIR

Figure 1(a) shows the effect of the pH value in the precipitation on the crystallinity of the $Nd_4(P_2O_7)_3$ catalysts and the effect of calcination temperature on the crystallinity of the NP-6 catalyst is shown in Fig. 1(b). The typical diffraction peaks of NP-4 were observed at 2θ = 28.3°, 30.8°, 33.8°, 36.7°, 41.8°, 46°, 48.5° which also appeared in the XRD patterns of the transition metal pyrophosphates calcined at 1,000 °C [23]. However, the diffraction peaks at 2θ = 26.5°, 52.5° appeared in the XRD patterns of $Nd_4(P_2O_7)_3$ catalysts were not observed in the

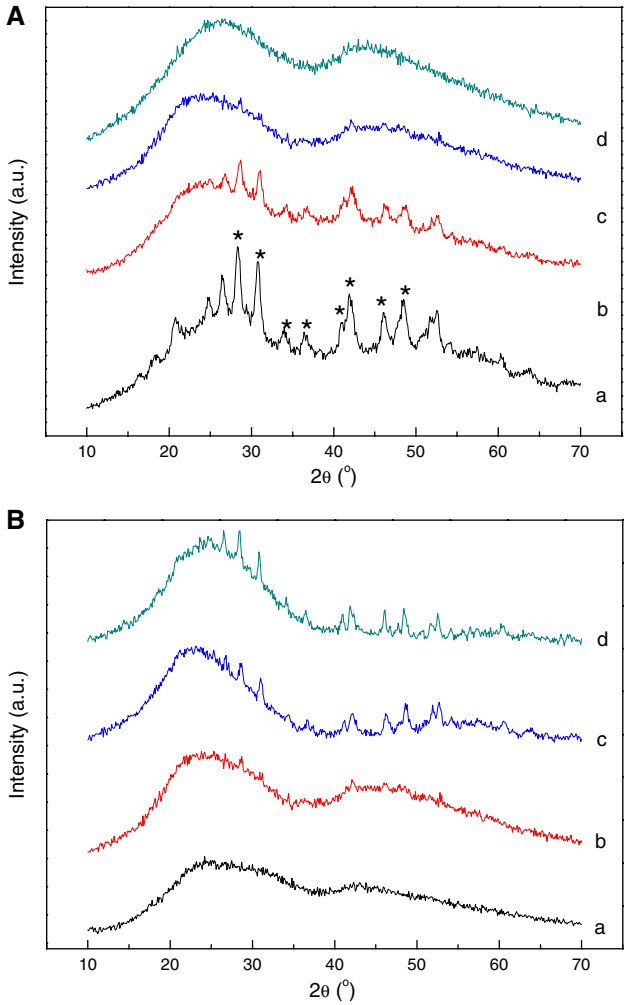

Fig. 1 XRD patterns of **a** (a) NP-4, (b) NP-5, (c) NP-6, (d) NP-7 calcined at 500 °C, **b** NP-6 catalysts calcined at (a) 400, (b) 500, (c) 600, (d) 700 °C

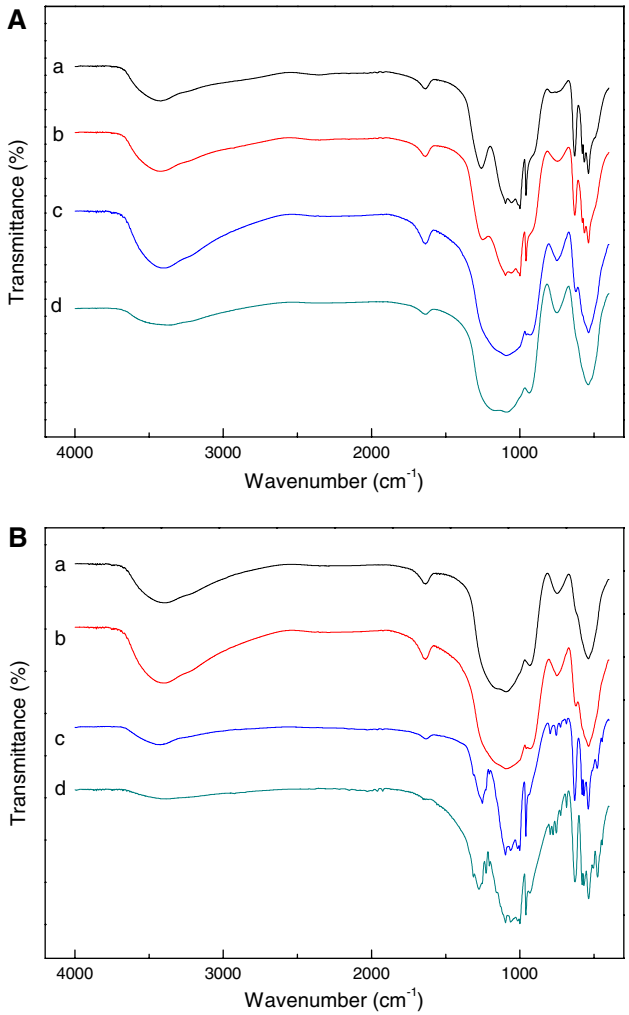

Fig. 2 FT-IR spectra of **a** (a) NP-4, (b) NP-5, (c) NP-6, (d) NP-7 calcined at 500 °C, **b** NP-6 catalysts calcined at (a) 400, (b) 500, (c) 600, (d) 700 °C

XRD patterns of the transition metal pyrophosphates. All the diffraction peaks of $Nd_4(P_2O_7)_3$ mentioned above were consistent with the $La_4(P_2O_7)_3$ and $Ce_4(P_2O_7)_3$ in our previously work [22]. As shown in Fig. 1(a), the intensity of all XRD peaks of the $Nd_4(P_2O_7)_3$ samples became weaker with pH value increasing from 4 to 7, which means that the samples posses the poorly ordered structure gradually with the increase of pH value in the precipitation. NP-7 appeared as an amorphous material, with no distinct X-ray diffraction detected from the sample. From Fig. 1(b), the diffraction peaks became clearer with the calcination temperature increased from 400 to 700 °C.

The FT-IR spectra of the $Nd_4(P_2O_7)_3$ catalysts are shown in Fig. 2, the bands at 770 cm^{-1} and 1,267 cm^{-1} appeared in NP-4, NP-5 (Fig. 2a) and NP-6 calcined at 600, 700 °C (Fig. 2b) which were attributed to $P_2O_7{}^{-4}$ and $P_4O_{12}{}^{-4}$ [24]. In our earlier report [22], the $P_2O_7{}^{-4}$ (polyphosphate anions) may play an important role in catalytic reaction over rare earth pyrophosphates. However, the band at 1,267 cm^{-1} did not appeared in NP-6, NP-7 (Fig. 2a) and NP-6 calcined at 400, 500 °C (Fig. 2b), this may be due to the amorphous structure of these samples which was also confirmed by the XRD patterns.

3.1.2 TG-DTA and BET

Figure 3 shows the TG-DTA curves of the as synthesized NP-6 catalyst, which was dried at 110 °C for 12 h. The weight loss on the TG curve closely matched the endothermic feature on the DTA curve, which should be attributed as an endothermic dehydration process. Most of the crystallization water in the hydrated precursor was removed by heating up to 500 °C. A sharp exothermic peak at 665 °C (Fig. 3) implies a transformation of the sample from its amorphous state to crystalline.

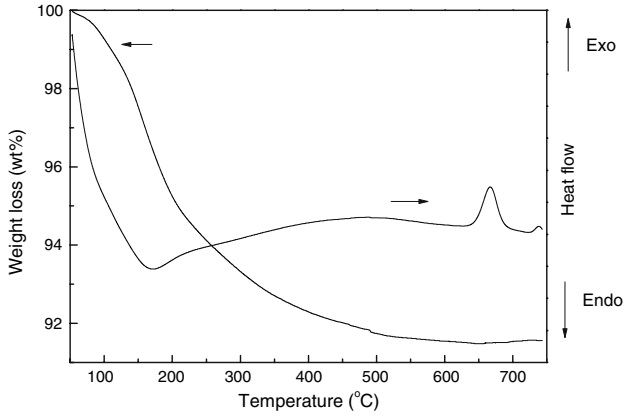

Fig. 3 TG-DTA curves of the as synthesized NP-6 catalyst

The specific surface areas of the NP-n ($n = 4$–7) catalysts and NP-6 catalysts calcined at 400–700 °C were listed in Tables 1 and 2, respectively. The specific surface areas of the NP-4, NP-5, NP-6 and NP-7 were 21.5, 19.3, 17.2 and 14.4 $m^2\ g^{-1}$, respectively, which decreased with the increase of pH value in the precipitation, which may be due to the smaller particle easily formed at the lower pH value. As shown in Table 2, increasing the calcination temperature resulted in continuous decreases surface area (from 44.2 to 5.5 m^2/g) of NP-6 catalyst.

3.1.3 NH_3-TPD Acidity Measurement

Figure 4 shows the NH_3-TPD profiles of (A) the NP-n ($n = 4$–7) catalysts calcined at 500 °C and (B) NP-6 catalysts calcined at 400–700 °C. From Fig. 4(a), there two main NH_3-TPD desorption peaks situated around 250 °C and 400 °C were observed on the samples, which were belonged to the weak acid site and strong acid site, respectively. With the pH value changed from 4 to 7, the intensity of NH_3 desorption peaks decreased gradually, which indicated that the acid amounts of both the two kinds of acid sites decreased with pH value increasing. However, the acid amounts of the strong acid decreased more seriously than the weak acid. When the catalyst precipitated at pH = 7, the NH_3 desorption peak of strong acid sites almost disappeared completely. As shown in Fig. 4(b), the intensity of NH_3 desorption peak at 250 °C denoting weak acid also decreased gradually with the increase of calcination temperature of NP-6 catalyst. It implies that lots of acidic sites were lost under the high calcination temperature. From above, both the catalyst precipitation condition and calcination temperature were crucial for the surface acidity of the $Nd_4(P_2O_7)_3$ catalyst.

3.2 Catalytic Reaction

3.2.1 Vapor-phase Dehydration of Glycerol -Over Some Rare Earth Pyrophosphates

Table 3 summarizes catalytic activities of some rare earth pyrophosphates in the vapor-phase dehydration of glycerol at 320 °C. As a decline of activity has been detected during the run, therefore, the activity was expressed hourly period according to the time on stream (TOS). The conversions of glycerol at the period of 2nd hour (TOS = 1–2 h for short in the text below, and so on) over most rare earth pyrophosphates all reached about 95%, and the selectivities of acrolein were all higher than 70% except $Ce_4(P_2O_7)_3$, $Lu_4(P_2O_7)_3$ and $Yb_4(P_2O_7)_3$. In contrast, after the reaction carrying out for the period of 8 h, the conversions of glycerol over most rare earth pyrophosphates decrease to about 76–89% and the selectivities of acrolein have a little increase compared with that of the initial 2 h. From Table 3, the catalysts $Nd_4(P_2O_7)_3$ and $Gd_4(P_2O_7)_3$ exhibited the highest selectivity (about 79 mol%) of acrolein. However, some catalysts such as $Ce_4(P_2O_7)_3$, $Lu_4(P_2O_7)_3$ and $Yb_4(P_2O_7)_3$ showed different catalytic performances compared with most rare earth pyrophosphates. The catalytic performances over $Ce_4(P_2O_7)_3$, $Lu_4(P_2O_7)_3$ and $Yb_4(P_2O_7)_3$ declined much more obviously, the glycerol conversion decreased seriously with the process time, and the selectivity of acrolein was <65% at the TOS = 8 h. $Ce_4(P_2O_7)_3$ catalyst is not suitable for the vapor-phase dehydration of glycerol due to the easier deactivation.

Table 1 Effect of pH value in the precipitation of $Nd_4(P_2O_7)_3$ catalyst on the product distribution in the vapor-phase dehydration of glycerol[a]

pH	BET (m^2/g)	Conv. (%)	Product selectivity (mol%)				
			Acrolein	Acetone	Hydroxylacetone	Allyl alcohol	Others[b,c]
4	21.5	84.9	60.4	0.6	5.9	0.5	32.6
5	19.3	93.6	81.9	0.8	7.3	0.8	9.2
6	17.2	96.4	82.7	0.6	9.5	0.7	6.5
7	14.4	80.7	80.2	0.9	7.8	0.9	10.2

[a] Reaction conditions: T = 320 °C, GHSV = 227 h^{-1}, TOS = 7–8 h

[b] Selectivity for others (mol%) = 100 − Total selectivity for all products identified

[c] Mostly polymer and coke

Table 2 Effect of the calcinaton temperature of NP-6 catalyst on the product distribution in the vapor-phase dehydration of glycerol[a]

Cal. Temp. (°C)	BET (m^2/g)	Conv. (%)	Product selectivity (mol%)				
			Acrolein	Acetone	Hydroxylacetone	Allyl alcohol	Others[b,c]
400	44.2	96.1	75.9	0.4	7.5	0.5	15.7
500	17.2	96.4	82.7	0.6	9.5	0.7	6.5
600	14.0	76.9	81.4	0.8	8.5	0.4	8.9
700	5.5	28.5	78.1	0.9	8.4	0.5	12.1

[a, b, c] Same as Table 1

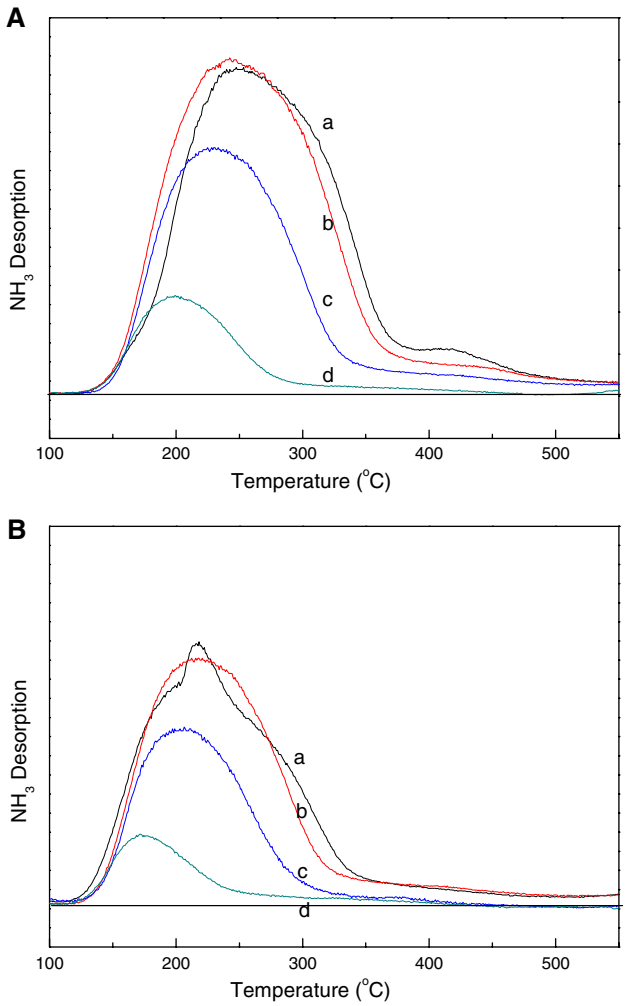

Fig. 4 NH_3-TPD profiles of **a** (a) NP-4, (b) NP-5, (c) NP-6, (d) NP-7 calcined at 500 °C, **b** NP-6 catalysts calcined at (a) 400, (b) 500, (c) 600, (d) 700 °C

Table 3 Catalytic performance of rare earth pyrophosphates catalysts for the vapor-phase dehydration of glycerol[a]

Catalyst	Catalyst charge (g)	t/h	Conversion[b] (%)	Selectivity[c] (%)
$La_4(P_2O_7)_3$	1.25	2	98.9	72.7
		8	76.2	78.5
$Ce_4(P_2O_7)_3$	1.18	2	99.8	39.7
		8	44.8	42.9
$Nd_4(P_2O_7)_3$	1.25	2	99.4	73.2
		8	87.2	79.9
$Sm_4(P_2O_7)_3$	1.30	2	99.6	74.2
		8	89.7	77.8
$Eu_4(P_2O_7)_3$	1.26	2	93.9	70.8
		8	83.1	78.5
$Gd_4(P_2O_7)_3$	1.24	2	98.2	75.7
		8	88.2	78.9
$Tb_4(P_2O_7)_3$	1.27	2	96.8	72.6
		8	87.6	78.8
$Ho_4(P_2O_7)_3$	1.24	2	95.4	71.3
		8	84.4	77.2
$Er_4(P_2O_7)_3$	1.33	2	97.2	72.8
		8	86.7	79.7
$Tm_4(P_2O_7)_3$	1.32	2	95.8	74.0
		8	87.0	77.8
$Yb_4(P_2O_7)_3$	1.30	2	78.6	58.4
		8	48.4	63.7
$Lu_4(P_2O_7)_3$	1.28	2	85.4	60.1
		8	58.5	64.4

[a] Reaction conditions: T = 320 °C, GHSV = 227 h^{-1}

[b] Glycerol conversion

[c] Selectivity for acrolein

As for $Lu_4(P_2O_7)_3$ and $Yb_4(P_2O_7)_3$, the lower conversion at the initial reaction is a fatal weak point. Various performances of rare earth pyrophosphates may be aroused from their different surface acidity. Zhang et al. [22] pointed out that different rare earth metal positive ions could result different surface acidity, which was confirmed by the NH_3-TPD profiles of $La_4(P_2O_7)_3$ and $Ce_4(P_2O_7)_3$. The distribution of main product from the dehydration of glycerol (TOS = 7–8 h) is presented in Table 4, hydroxylacetone was the main byproduct, but the selectivity of hydroxylacetone was no more than 10 mol% for all rare earth pyrophosphates. Acetone and allyl alcohol were also detected in a small amount. Moreover, a large amount of unidentified products (11.4–44.1%) were found, it should be mostly polymer and coke.

Table 4 Distribution of product for the vapor-phase dehydration of glycerol over the rare earth pyrophosphates catalysts[a]

Catalysts	Conversion (%)	Product selectivity (mol%)				
		Acrolein	Acetone	Hydroxylacetone	Allyl alcohol	Others[b,c]
$La_4(P_2O_7)_3$	76.2	78.5	0.2	7.3	0.6	13.4
$Ce_4(P_2O_7)_3$	44.8	42.9	0.7	9.9	2.4	44.1
$Nd_4(P_2O_7)_3$	87.2	79.9	0.1	4.3	0.6	15.1
$Sm_4(P_2O_7)_3$	89.7	77.8	0.2	5.8	0.7	15.5
$Eu_4(P_2O_7)_3$	83.1	78.5	0.5	6.2	0.8	14.0
$Gd_4(P_2O_7)_3$	88.2	78.9	0.2	7.5	0.8	12.6
$Tb_4(P_2O_7)_3$	87.6	78.8	0.7	6.5	0.9	13.1
$Ho_4(P_2O_7)_3$	84.4	77.2	0.6	6.8	0.9	14.5
$Er_4(P_2O_7)_3$	86.7	79.7	0.6	7.4	0.9	11.4
$Tm_4(P_2O_7)_3$	87.0	77.8	0.5	7.8	0.8	13.1
$Yb_4(P_2O_7)_3$	48.4	63.7	0.3	3.8	1.8	30.4
$Lu_4(P_2O_7)_3$	58.5	64.4	0.4	6.8	1.0	27.4

[a] Reaction conditions: T = 320 °C, GHSV = 227 h^{-1}, TOS = 7–8 h

[b] Selectivity for others (mol%) = 100 − Total selectivity for all products identified

[c] Mostly polymer and coke

As we known, the acid strength and acid amount of the catalyst were significant for the catalytic activity, inappropriate acidity of catalyst may cause poor results, such as lower selectivity accompanied with severe coke deposition, and short catalyst lifetime. Rare earth pyrophosphates exhibited higher conversion and longer lifetime than other catalysts in vapor phase Beckmann rearrangement of cyclohexanone oxime [22], which was due to the appropriate weak surface acidity and surface hydrophobicity of the catalyst. In present work, the appropriate surface of the rare earth pyrophosphates is also the key factor for the excellent catalytic performance in the dehydration of glycerol to acrolein. Polyphosphate anions play an important role in the acidity and the catalytic activities of rare earth pyrophosphates, which could be illuminated by the NH_3-TPD profiles of rare earth pyrophosphate, rare earth tripolyphosphate and rare earth phosphate exhibited in our previous work [22].

3.2.2 *Effect of PH Value (in the Range of 4–7) in the Preparation of $Nd_4(P_2O_7)_3$ Catalysts on the Vapor-phase Dehydration of Glycerol*

Figure 5 depicts the time dependent glycerol conversion and acrolein selectivity over NP-n (n = 4–7) catalysts. As shown in Fig. 5, the conversions of glycerol over the four catalysts followed the order: NP-4 > NP-5 > NP-6 > NP-7 during the initial 2 h reaction. However, after the reaction was performed for 8 h, the conversion of glycerol followed: NP-6 > NP-5 > NP-4 > NP-7. The decrease in the glycerol conversion over the four catalysts was in the order: NP-4 > NP-5 ≈ NP-7 > NP-6. Thus, the conversion of glycerol over NP-4 catalyst decreased more quickly with time courses than the other three catalysts, and the selectivity of acrolein was stabilized at only about 60% during the 8 h reaction. Table 1 shows the product distribution over the NP-n (n = 4–7) catalysts for the vapor-phase dehydration of glycerol (TOS = 7–8 h). With the change of precipitation condition, the selectivity of all the identified byproducts had a little change. The selectivity of hydroxylacetone reached 9.5% over NP-6. However, the selectivity of unidentified products (mostly polymer and coke) decreased obviously over the catalysts by changing the pH value from ~4 to 6–7 in the precipitation.

Considerable carbon deposits were formed on the $Nd_4(P_2O_7)_3$ catalysts during the catalytic reaction. TPO characterization of the used catalysts (after 8 h TOS) was conducted with flowing air in the TG-DTA mode; the results are compared in Fig. 6. The weight loss below 250 °C on the TG curves (Fig. 6a) was due to the elimination of adsorbed water and evaporable organic compounds. The weight loss in the range of 300–420 °C was accompanied by a broad, strong exothermic peak on the DTA curves in the same temperature range, it is owing to the removal of organic residue and easily oxidizable carbonaceous species such as amorphous type of coke precursors. Above 430 °C, the large weight loss can be assigned to the oxidation of carbon deposits which may be graphitic carbon. The amounts of carbonaceous deposits measured from the TG curves were plotted in Fig. 7 as a function of pH value in the precipitation of catalyst. From Fig. 7, the formation of coke on NP-4 catalyst is more severely than the other three catalysts, this could be attributed to the more strong acid sites of NP-4. The carbon

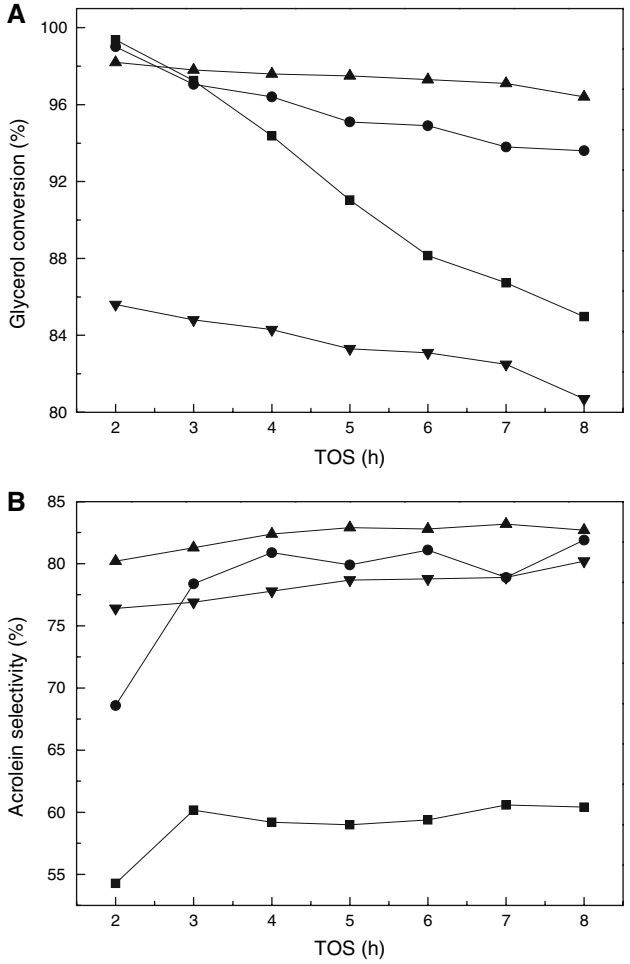

Fig. 5 Time courses of **a** glycerol conversion and **b** acrolein selectivity over: (■) NP-4, (●) NP-5, (▲) NP-6, (▼) NP-7

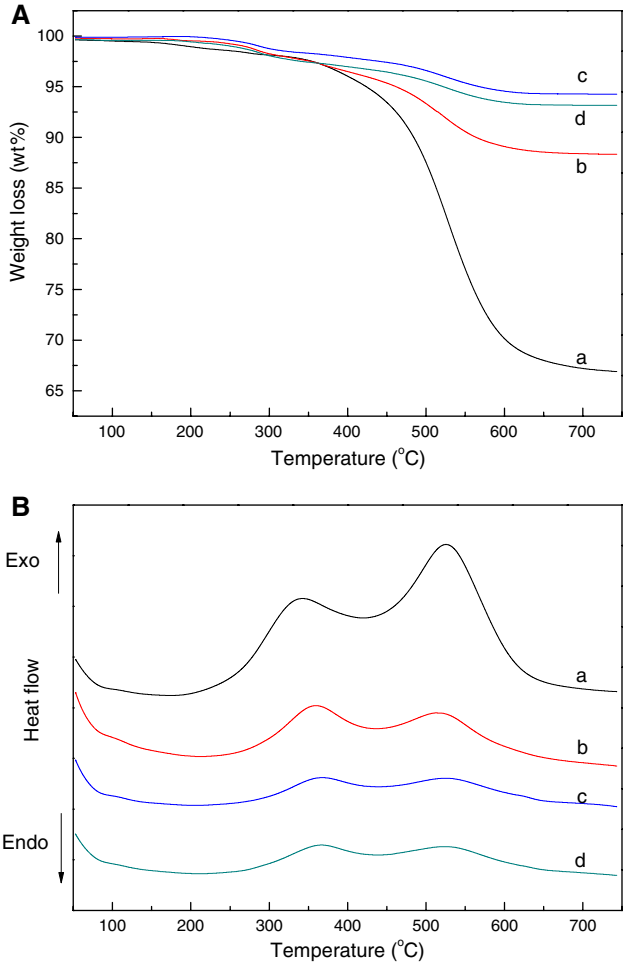

Fig. 6 **a** TG and **b** DTA curves of the used $Nd_4(P_2O_7)_3$ catalysts: (a) NP-4, (b) NP-5, (c) NP-6, (d) NP-7 calcined at 500 °C

amount on catalyst surface is given in the following order: NP-4 > NP-5 > NP-7 > NP-6.

From the NH_3-TPD profiles of the NP-n ($n = 4$–7) catalysts (Fig. 4a), NP-4 catalyst showed more amounts of strong acid sites more than the other three. Moreover, NP-4 catalyst coked most severely indicated by TG-DTA (Figs. 6 and 7), and the selectivity of the other products was also much higher than the others (Table 1). This could be due to the strong acid resulted side reactions among the reactant and the products such as acrolein, hydroxylacetone and allyl alcohol, etc. With the increasing of pH value in the precipitation, the acid amount of the strong acid reduced severely, thus the catalytic performances of the catalysts were improved. The glycerol conversion over NP-5 catalyst decreased slightly and the selectivity of acrolein was improved to more than 75%. NP-6 catalyst showed the best performance in the vapor-phase dehydration of glycerol reaction, the conversion of glycerol only

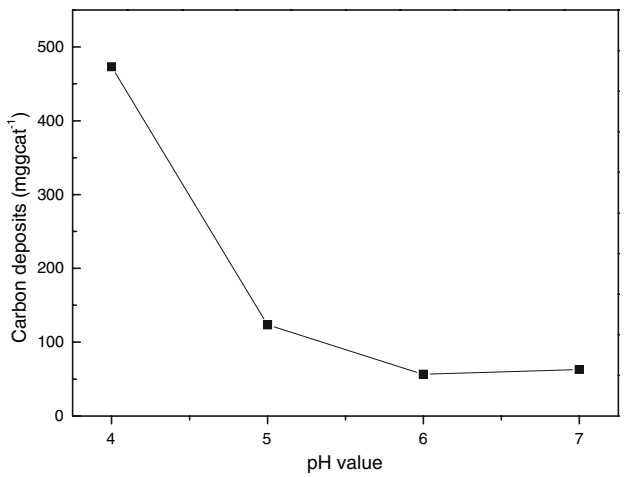

Fig. 7 Effect of the catalysts precipitation condition of pH value on the amount of carbon deposits over the used $Nd_4(P_2O_7)_3$ catalysts (TOS = 7–8 h)

had a little decrease with time courses (96.4% at TOS = 8 h), at the same time the selectivity of acrolein maintained steady about 82.7% in all reaction time, and the amount of coke deposits was reduced obviously. This could be due to the large lost of strong acid sites of the sample. While over the NP-7, low conversion of glycerol at the initial of the reaction (Fig. 5) is connected with the largely reduced of the amount of the weak acid site. As mentioned above, the coke deposits were caused by the strong acid sites of the catalyst, and the weak acid sites were considered as the active center in the vapor-phase dehydration of glycerol. The appropriate surface acidity of the rare earth pyrophosphates was crucial for the double dehydration reaction of glycerol, and the catalysts with weak acidity sites were more effective for glycerol dehydration and the formation of desired acrolein. A suitable pH value for the precipitation in the preparation of rare earth pyrophosphates catalyst could effectively improve the catalytic performance and prolong the lifetime of the catalyst.

3.2.3 *Effect of Calcination Temperature on the Performance of NP-6 Catalyst*

Figure 8 shows the effect of the calcination temperature of NP-6 on glycerol conversion and acrolein selectivity at TOS of 1–2 h and 7–8 h. As shown in Fig. 8(a), the glycerol conversion decreased with the increasing of calcination temperature and more seriously in the time courses over the catalyst calcined at 700 °C. From Fig. 8(b), the selectivity of acrolein increased with calcination temperature first, and reached a maximum (82.7%) at 500 °C, then declined with further increase of calcination temperature. After the reaction carrying out for 8 h, the NP-6 catalyst calcined at 500 °C exhibited the best catalytic performance, the glycerol conversion reached 96.4 mol% and the acrolein selectivity reached 82.7 mol%. The effect of calcination temperature on the product distribution over NP-6 catalyst for the vapor-phase dehydration of glycerol (TOS = 7–8 h) was exhibited in Table 2. The selectivity of unidentified products decreased largely with the calcination temperature increased from 400 °C to 500 °C at first, then followed by increased to about 12.1% when the catalyst calcined at 700 °C.

The TG-DTA curves of the used NP-6 catalysts calcined at 400–700 °C are shown in Fig. 9 and the amounts of coke deposits measured from the TG curves are plotted in Fig. 10. As shown in Fig. 10, whereas the general trend is that catalysts calcined at low temperatures coked more severely than catalysts calcined at high temperatures. Moreover, the results of the coke formation on the NP-6 calcined at different temperature are consistent with the variation of acidity.

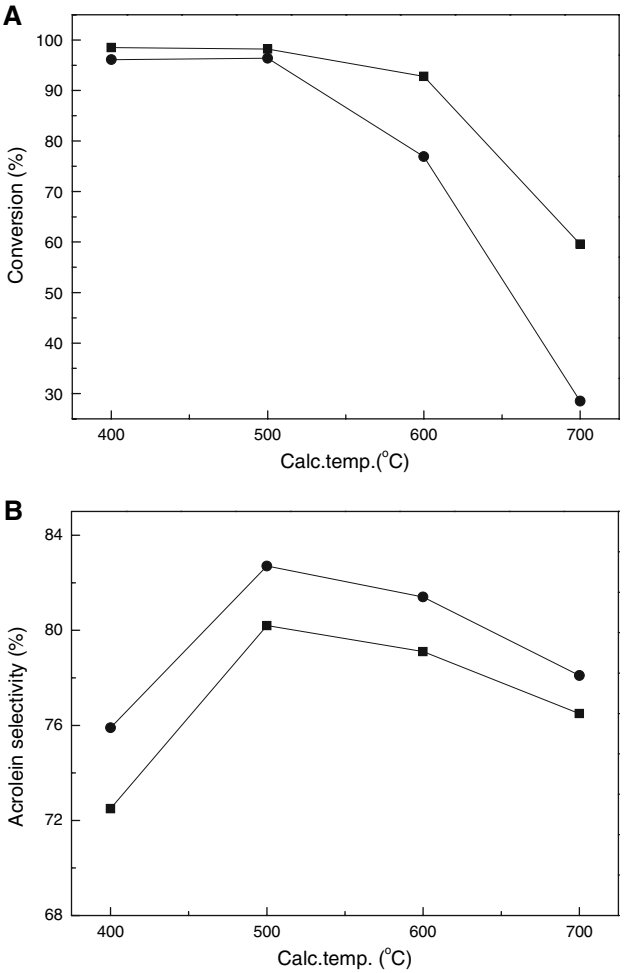

Fig. 8 Effect of the catalyst calcination temperature on **a** glycerol conversion and **b** acrolein selectivity over NP-6 at (■) TOS = 1–2 h and (●) TOS = 7–8 h

The effect of calcination temperature of NP-6 catalyst on its catalytic performance is directly related to the amount of surface weak acid sites and the BET surface areas. The catalysts calcined at 400 and 500 °C were amorphous, as indicated by the XRD data and TG-DTA (Figs. 1b and 3), and also demonstrated the more weak acid sites than other catalysts (Fig.4b) and the high surface areas (Table 2). The catalysts prepared by calcination at high temperatures (such as 700 °C) exhibited quite low surface area, which also showed the least amounts of surface acidity. Moreover, the amounts of carbon deposits were also consistent with the surface acidity and the BET surface area of the catalysts. Furthermore, the unidentified components in the product over the NP-6 catalyst calcined at 500 °C were less than the samples calcined at higher or lower than 500 °C. From above, it can be seen that the catalyst calcined at 500 °C is optimum to obtain the most appropriate surface acidity for the vapor-phase dehydration of glycerol.

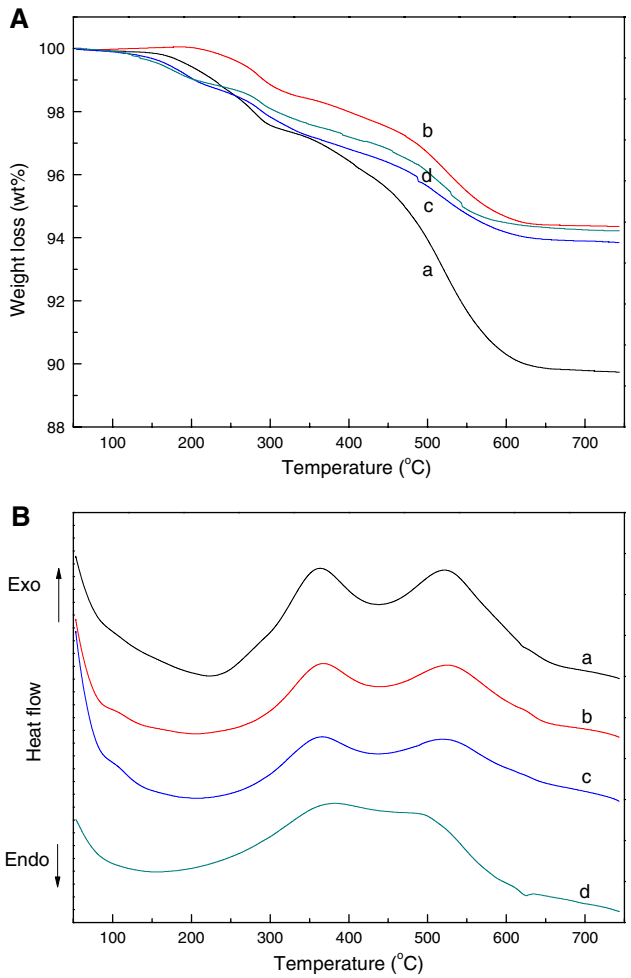

Fig. 9 **a** TG and **b** DTA curves of the used NP-6 catalyst calcined at: (a) 400, (b) 500, (c) 600, (d) 700 °C

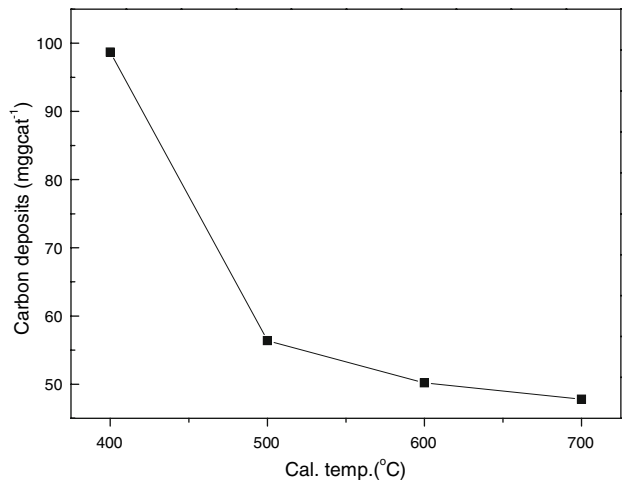

Fig. 10 Effect of the catalysts calcination temperature on the amount of carbon deposits over the used NP-6 catalyst (TOS = 7–8 h)

Though a stable selectivity of acrolein >82 mol% was obtained from the dehydration of glycerol over $Nd_4(P_2O_7)_3$ catalyst (pH = 6, calcined at 500 °C, TOS = 8 h), there still great improvement is needed before put it into a practical usage. For example, Tsukuda et al. found that silicotungstic acid supported on silica with mesopores of 10 nm showed the highest catalytic activity with the selectivity of acrolein >85 mol% [13]. Thus, seeking for an appropriate support for rare earth pyrophosphates may effectively reduce the disparity with the commercial catalyst.

4 Conclusion

Rare earth pyrophosphates showed high acrolein selectivity and long lifetime in the vapor-phase dehydration of glycerol to produce acrolein. The surface weak acidic sites formed by polyphosphate anions were considered as the active center in this work. The influence of precipitation condition and calcination temperature was not ignored, through optimizing the proper selection of precipitation condition and the calcination temperature, the excellent catalytic performance was achieved over $Nd_4(P_2O_7)_3$ catalyst (prepared at pH = 6, calcined at 500 °C).

Acknowledgments We thank the Ministry of Science and Technology of China (973 program 2003CB615805) and the National Natural Science Foundation (20573103) for the support of this research.

References

1. Klass DL (1998) Biomass for renewable energy, fuels and chemicals. Academic, San Diego, p 1
2. Centi G, Perathoner S (2003) Catal Today 77:287
3. Van Bekkum H, Gallezot P (2004) Top Catal 27:1
4. Huber GW, Dumesic JA (2006) Catal Today 111:119
5. Adkins H, Hartung WH (1941) Org Synth Coll 1:15
6. Neher A, Haas T, Arntz D, Klenk H, Girke W (1995) U.S. Patent 5,387,720
7. Schwenk E, Gehrke M, Aichner F (1933) U.S. Patent 1,916,743
8. Ramayya S, Brittain A, DeAlmeida C, Mok W, Antal MJ (1987) Fuel 66:1364
9. Ott L, Bicker M, Vogel H (2006) Green Chem 8:214
10. Watanabe M, Iida T, Aizawa Y, Alda TM, Inomata H (2006) Bioresour Technol 98:1285
11. Chai S, Wang H, Liang Y, Xu B (2007) Green Chem 9:1130
12. Chai S, Wang H, Liang Y, Xu B (2007) J Catal 250:342
13. Tsukuda E, Sato S, Takahashi R, Sodesawa T (2007) Catal Commun 8:1349
14. Atia H, Armbruster U, Martin A (2008) J Catal 258:71
15. Aït-Lachgar-Ben Abdelouahad KA, Roullet M, Brun M, Burrows A, Kiely CJ, Volta JC, Abon M (2001) Appl Catal A Gen 210:121
16. Carrara C, Irusta S, Lombardo E, Cornaglia L (2001) Appl Catal A Gen 217:275
17. Marcu I-C, Sandulescu I, Millet J-MM (2002) Appl Catal A Gen 227:309
18. Marcu I-C, Sandulescu I, Millet J-MM (2003) J Mol Catal A Chem 203:241
19. Marcu I-C, Sandulescu I, Millet J-MM (2008) Appl Catal A Gen 334:207

20. Xiong YL, Xiao DH, Li J, Yang XG, Wu Y (2005) Z Phys Chem 219:1121
21. Xiong YL, Li J, Yang XG, Wu Y (2006) Z Phys Chem 315
22. Zhang Z, Li J, Yang XG (2007) Catal Lett 118:300
23. Onoda H, Kojima K, Nariai H (2006) J Alloy Comp 568:408
24. Corbridge DEC, Lowe EJ (1954) J Chem Soc 493:4555